Dynamic Measurement of Nanoflows: Realization of an Optofluidic Flow Meter to the Nanoliter per Minute Scale

Gregory A. Cooksey*[1], Paul N. Patrone[2], James R. Hands[1], Stephen E. Meek[1,3], Anthony J. Kearsley[2]

[1]Microsys. and Nanotech. Division and [2]Appl. and Comp. Math. Division, National Institute of Standards and Technology (NIST), Gaithersburg, MD 20899, USA. [3]Biotechnology Program, Montgomery College, Germantown, MD 20876, USA.

ABSTRACT: The ultimate performance of flow-based measurements in microfluidic systems is currently limited by their accuracy at the nanoliter-per-minute scale. Improving such measurements (especially in contexts that require continuous monitoring) is challenging because of constraints associated with shrinking system geometries and limitations imposed by making precise measurements of smaller quantities in real time. A particularly interesting limit is the relative uncertainty as flow approaches zero, which diverges for most measurement methods. To address these problems, we have developed an optofluidic measurement system that can deliver and record light in a precise interrogation region of a microfluidic channel. The system utilizes photobleaching of fluorophore dyes in the bulk flow and can identify zero flow to better than 1 nL/min absolute accuracy. The technique also provides an independent method for determining non-zero flow rates based on a robust scaling relationship between the fluorescence emission and flow. Together, these two independent approaches enable precise measurement of flow to within 5% accuracy down to 10 nL/min and validation of flow control to within 5 % uncertainty down to 2 nL/min. We also demonstrate that our technique can be used to extend a calibrated flow meter well below its specified range (e.g., 500 nL/min) and to make dynamic measurements of similar relative uncertainties to the calibrated meter, which would have otherwise expanded significantly in this regime.

Flow measurement is fundamental to validating the performance of microfluidic systems. For example, techniques such as high-performance liquid chromatography and drug perfusion all require accurate control of microflows.[1–4] In addition, systems that operate in the microscale regime use flow measurement to calculate shear, control formation of microdroplets[5] or concentration gradients,[6] perform continuous flow separations,[7] and ensure mass transfer of nutrients and drugs in medical and biotech applications.[8,9] However, next-generation microfluidic and lab-on-a-chip applications will require ever more accurate, in situ, and continuous measurements of flow that are not achievable using conventional methods (e.g., less than 1 μL/min). Thus, new methods are needed to improve sensitivity and decrease uncertainty of ultralow flow measurements.

State of the art for low-flow metrology has primarily been achieved through careful miniaturization of gravimetric methods and control of environmental conditions. Such approaches have achieved high-precision flow measurements on the order of 1 μL/min,[10] and further optimization has allowed for measurement of >10 nL/min to within a few percent error (Table 1).[11,12] Uncertainties as low as 5% at 5 nL/min have been achieved with 5 min integration time.13 However, these and related techniques14−17 are increasingly constrained by practical limitations associated with geometry, temperature, or interfacial properties at the microscale. Moreover, they suffer from an inability to simultaneously achieve both real-time and high-precision measurement. Therefore, further improvement in low-flow measurements may require a combination of both advanced engineering techniques and new conceptual approaches that leverage our understanding of fluid behavior at the microscale.

We report here the development and testing of an optofluidic flow meter that includes two novel and independent techniques to aid in the measurement of very small liquid flow rates. Conceptually, our system utilizes fluorophore bleaching rate[18–22] at a small laser interrogation region in a microchannel as a natural time scale to continuously determine the rate of bulk flow. The integrated intensity of fluorophores as they pass through the interrogation region (and bleach) decreases as a function of light dosage. As flow rates are reduced, the dwell time of fluorophores in the laser increases, which, like increasing laser power, leads to more bleaching. We use this relationship between fluorescence efficiency and dosage (power and time) to trace out a master curve that when calibrated at a single flow rate can be used to determine any unknown flow rate from the corresponding measurement of fluorescence efficiency for a given laser power. The mathematical analysis supporting the robustness of the scaling method to unknowns, such as the system geometry, has been described in a preceding manuscript.[23] Interestingly, we found that this approach can scale flow measurements accurately down to the nanoliter-per-minute range, but it also yields an independent measurement of zero flow having an absolute uncertainty of 0.2 nL/min or less. Importantly, this capability allows us to drastically improve the accuracy of existing flow meters and controllers. To illustrate this, we (i) demonstrate scaling a meter with 5% uncertainty at ≈500 nL/min to 10 nL/min with the same uncertainty using gravity-based control and (ii) illustrate flow control to 5% uncertainty at 2 nL/min.

We find that the accuracy of two reference measurements—one using a calibrated flow meter and another at zero flow—is the main limiting factor in both calibrating our device and validating its operation. Because commercial flow meters are accurate in the 1 μL/min range, formulation of a zero-flow measurement is the novel element that enables success of our approach.

Table 1. Comparison of common methodologies for microscale liquid flow measurement

Method	Practical Lower Limit (nL/min)	Best Uncertainty	Time Resolution	Advantages	Limitations	Reference
Mass balance (gravimetric)	10	5 nL/min; < 1% for > 100 nL/min	minutes	Traceable	Evaporation, slow, surface and buoyant forces	10-12
Front tracking	5	5 % (0.025 nL/min)	minutes	Traceable	One measurement, difficult to control surface chemistry	13, 14
Fluorescence bleaching and imaging	100*	5 %†	Seconds to minutes	Dynamic, High SNR	Requires calibration, known geometry	21, 22, 30-33
Thermal dilution	70	10 %	0.1 s	Real time, in-line	Requires calibration; heats fluid; Small dynamic range	15
PTV	2	2 %	minutes	Full velocity profile	Computationally intensive, Particle/flow interaction	5, 16
Cantilever deflection	5	N.D.	seconds	Scalable, multifunctional	Requires calibration, Complicated fabrication	17
Pressure sensing membrane	0.002	N.D.	minutes	Very low range	Sensor drain after each measurement; custom fabrication; temp. sensitivity; must be at the end of flow path	34
This paper	0.1	Demonstrated to 5% down to 10 nL/min; determined by calibration method	0.1 s	Real-time, high SNR, scales down other methods, ability to precisely find zero flow; moderate dynamic range	Requires calibration, laser, and optical detectors, and fluorophore	23

*estimated from 1 mm/s linear velocity in 50 μm diameter capillary. † Best uncertainty is not described in the references, but repeatability on the order of 1 %[21] and 4 %[22] are demonstrated. Additional uncertainties are likely higher. N.D. = not described, but likely not better than 10 % based on data presented in the references. PTV = particle tracking velocimetry. SNR. = signal-to-noise ratio.

This work bears similarities to other techniques that use photobleaching to determine liquid flow rates.[21,22] However, the methods presented herein are distinct in that they (1) incorporate a robust optical system, (2) introduce a novel method to determine zero flow, (3) leverage mathematically (i.e., provably) rigorous light-dosage scaling and symmetry relationships (as opposed to empirical models) that do not require knowledge of the system geometry,23 and thereby (4) enable a robust uncertainty analysis, which extends measurements into heretofore unachievably refined low-flow regimes.

THEORY, DESIGN, AND METHODS

Conceptually, the description and operation of our optofluidic flowmeter (shown in **Figure 1**) is straightforward, although the underlying mathematical analysis is quite complex. Here, we provide a brief description of the operating principles, with an emphasis on the physical interpretation of the mathematics. We also provide a conceptual overview of the zero-flow measurement, which is not covered in our preceding manuscript.[23]

Principles of Operation. On average, the total number of photons emitted by a fluorescent molecule before bleaching is a constant, regardless of the rate at which excitation light is absorbed.[18] In a microfluidic channel the fluorescence rate depends on the intensity of excitation light and the fluorophore dwell time in that light. Thus, for fixed laser power, the distance that a flowing unbleached fluorophore survives into the interrogation region (in the *z*-dimension) is proportional to v_v, the volumetric flow rate, provided each dye molecule remains on a single streamline. In other words, decreasing the flow rate decreases the emitted fluorescence intensity, *I*, of the entire system. If bleaching rate is a monotonically increasing function $f(p)$ of the laser power,[20] and if $f(p)$ is normalized to have units of power, then dimensional analysis tells us that the energy density (i.e., photon number/area) delivered to a fluorophore on a fixed streamline is proportional to the dosage $\xi = f(p)/v_v$. Further analysis, which is more explicitly described in our complementary paper,[23] leads to a relationship that assures each measured fluorescence efficiency (emission/excitation power or $\hat{I}(\xi) = I/p$) is associated with a unique dosage.

By itself, this efficiency-dosage relationship only allows flow measurement on a relative scale. Determining the absolute scale requires calibration of the device. Specifically, we use a calibrated flow meter to measure some v_v at the lower limit of the latter's capability. Knowing v_v and $f(p)$, we vary the power and map out an efficiency curve $\hat{I}(\xi)$. To measure lower flow rates, we fix p and change v_v to an unknown value. Having previously mapped out $\hat{I}(\xi)$, we now relate the efficiency to a dosage, and therefore to a specific value of v_v. Importantly, this approach has the benefit of preserving the relative uncertainty of the calibration flow meter, but at much lower flow rates. For more details on the mathematical modeling and analysis, see manuscript by Patrone et al.[23]

Zero-flow determination. Photobleaching of fluorescein as it crosses the interrogation region motivates an elegant solution to the problem of measuring zero flow. Specifically, if we assume a symmetric illumination about the center of the interrogation region, an image of fluorescence appears dark in the center, since the dye is bleached except for diffusion of unbleached fluorophore from either end of the region. From symmetrically placed collection waveguides around the interrogation region, in the limit that $v_v \to 0$, *I* should attain a critical value.

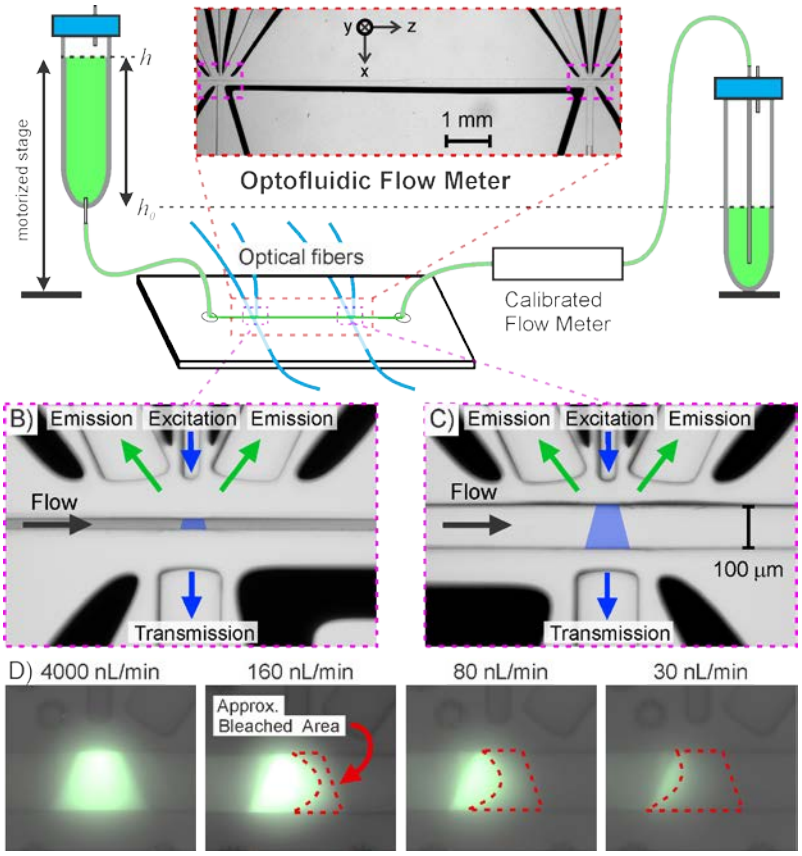

Figure 1. (A) Schematic showing optofluidic device with fluidic connections. The height of the source reservoir (h) compared to the collection reservoir (h_0) determines the pressure for flow through the optofluidic device and commercial flow meter. Inset shows image of narrow and wide regions (separated 9 mm in z dimension, as shown in A) along a single flow path. Images show narrow (B) and wide (C) channel interrogation regions with arrows indicating direction and primary wavelength (blue = 488 nm, green = 520 nm) of excitation, emission, and transmission light in waveguides. Shaded blue zone marks the approximate excitation area within the interrogation region. Channels along each waveguide were filled with black PDMS (Sylgard 170) to block stray excitation light. (D) Demonstration of photobleaching as a function of flow rate. At high flow rates (low dosages), fluorescein is not bleached, and fluorescence fills the full laser illumination zone across the microchannel (left). Photobleaching increases near the walls and increasingly closer to the entrance of flow the interrogation region as flow decreases (images from left to right). Flow is left to right. Channel widths are 100 µm (C, D) and 25 µm (B). All structures are ≈ 80 µm tall (in y dimension).

Deviation around zero is then detected by polarity changes in the fluorescence pattern (by microscopy) or intensity shift from one waveguide to another (see **Figure 2**).

Device Design Principles. Operation of the flow meter assumes laminar flow, the existence of which can be assessed using the Reynolds number (*Re*). For a microchannel with a constant cross section having width (w) ≈ height (h) ≈ 100 µm and total length, L (in z) » w, flows ranging from 1 nL/min to 10 µL/min have *Re* < 1, which is well within the bounds of laminar flow (*e.g.*, *Re* « 2300) (see **Suppl. Info. 1**). In fact, such flows are Poiseuille, and consequently, the shape of the flow profile is invariant for all v_v in our domain of interest. In other words, a fluid packet on any streamline has a linear velocity proportional to v_v, as required.

Diffusion of fluorophores also constrains device fabrication. Specifically, operation of the device requires that diffusion be negligible compared to pressure-driven flow, since fluorophores must remain on a single streamline. The relative magnitude of these effects is encoded in the Peclet number $Pe = t_D/t_C$, where t_D and t_C are the characteristic diffusion and convection times, respectively. For our purposes, we require Pe » 1. For fluorescein (diffusion coefficient ≈ 430 µm²/s), the Peclet number associated with a given dimension can be expressed as $Pe \approx 38V/W$, where V is a numerical value (in nanoliters per minute) and W is the corresponding value of the characteristic dimension (in micrometers). We conservatively pick W as the largest of w, h, and L_z, the length of the interrogation region. We expect deviation from theory (due to diffusion) to go as roughly $1/Pe$,[23] so we consider it reasonable to maintain Pe > 10 or V/W > 0.26.

For a device whose largest characteristic dimension is 100 µm, 25 nL/min represents an anticipated lower bound (≈ 10 % uncertainty) on operation of the device, while 2.5 nL/min would be a rough lower bound on the capabilities of a device whose characteristic dimension is 10 µm. **Figure S1A** summarizes the theoretical performance of a device as a function of its characteristic dimension. See the **Results** for refinement of performance estimates given practical observations.

We emphasize that no particular shape or precise length of the interrogation region (aside from the aforementioned bounds) is assumed, since the measurement makes no explicit reference to these. Moreover, the physics of bleaching,

fluorescence [aside from knowledge of $f(p)$], light absorption, geometric factors associated with the waveguides, etc. do not enter the analysis underlying the measurement. Indeed, it is entirely possible that the excitation light may be largely absorbed by the fluorophores, with very little transmitted to the far side of the channel, and yet the measurement can still be performed. See Patrone et al.[23] for more details. Thus, most details of the construction and operation that we pursue can be modified, provided that: (i) the approximate length-scale bounds are satisfied; and (ii) the setup enables accurate measurement of the input and output light intensities.

The sensitivity of the system to different flow velocities (for a given volumetric flow) was tested by creating two different interrogation regions in the device: a 100 μm wide channel and a narrowed 25 μm wide channel (**Figure 1**). For a given microfluidic flow rate, the wider channel will have a slower linear velocity and fluorophores will be more susceptible to photobleaching. The narrower channel will have faster relative velocities and fluorescence should be maintained in the channel at higher dosages of laser power (or slower volumetric flow rates). Thus, the narrower region is expected to be more sensitive to measurements of smaller volumetric flow rates.

Materials, fabrication, and measurement procedure

Dislcaimer: Identification of commercial products does not imply recommendation or endorsement by the National Institute of Standards and Technology (NIST). The materials and equipment used may not necessarily be best for purpose.

Optofluidic devices were created using photolithography and soft lithography methods.[24,25] Patterns were made on silicon wafers spin coated with SU8 (SU-8 2075, Microchem). These masters were directly written using a maskless aligner (MLA 150, Heidelberg Instruments) at the Center for Nanoscale Science and Technology at NIST. Exposed wafers were developed and derivatized with trichloro(1H,1H,2H,2H-perfluorooctyl)silane (Sigma-Aldrich).

Devices were cast in poly(dimethylsiloxane) (PDMS) (Sylgard 184, 10:1, Dow Corning) by pouring PDMS over the master wafer and curing overnight at 70 °C. A flat piece of PDMS from the wafer served as the substrate for the bottom of the microchannels. Inlet ports were made in the channel-forming layer using a 0.75 mm Harris Micro-Punch. Following rinsing with ethanol and water, the PDMS layers were treated with oxygen plasma (Plasma Preen, Plasmatic Systems Inc) for 30 s and pressed together. Light-blocking channels were filled with opaque PDMS (Sylard 170, 1:1, Dow Corning) and cured for 1 h at 70 °C. Next, the waveguide channels of the device were filled with optical adhesive (Norland 88, Norland Products) and degassed. Stripped and cleaved optical fibers (FG105UCA, Thorlabs) were inserted into the tapered ends of the waveguide channel followed by curing of optical adhesive with UV light for 2 h (UVP Blak-Ray High Intensity Lamp). Inlet and outlet reservoirs were connected to devices with Tygon tubing (S3, 0.89 mm inner diameter, 2.57 mm outer diameter, Cole Parmer) and blunt 21G needles with 90-degree bends (McMaster-Carr).

Optical fibers exiting the waveguides were connected to either a fiber-coupled diode laser (LuxX 488 nm, 60 mW, Omicron-Laserage), which served as the excitation light source, or photodetectors (918D-SL-OD2R, Newport Corp.) coupled to a power meter (2936-R, Newport Corp.). Photodetectors measured transmitted (excitation) and emitted fluorescent light (with Chroma ET450/50 filter in front of detector), respectively. A nominal 10 % transmittance neutral density filter (Chroma Technology Corp) was added to the optical path to extend the power range of our system to lower levels. Emission collecting waveguides were symmetrically positioned upstream and downstream on the side on the same side of the channel as the excitation waveguide and tilted approximately 40% from the excitation axis. Transmitted light was collected in a waveguide across the microchannel that was widened to account for dispersion of light from the source. Measurement of transmitted light was used to estimate the excitation laser power used in the dosage and fluorescence efficiency calculations.

Flow measurements were conducted using 20 or 50 μmol/L fluorescein in buffer (30181, Sigma Aldrich; dissolved in phosphate buffered saline, pH 7.4, Thermo Fisher). Flow rates were controlled via gravity with a reservoir attached to a motorized stage having an accuracy of roughly 0.05 mm (LTS300, Thor Labs). A NIST-calibrated[11] commercial flow meter (LG16-0150D, Sensirion AG, Staefa ZH, Switzerland) was connected in series as the calibration source for the optofluidic flow meter.

To create the calibrated dose-response curve, fluorescence emission and excitation power were recording during scans of laser power in 5 or 10 % increments at maximum flow rate, which was achieved at the maximum extent of the scanning stage (300 mm) and dependent on the fluidic resistance of the entire flow system (see **Suppl. Info. 2**). Typically, maximum flow was on the order of 1000 nL/min. To validate that laser power and flow rate^{-1} are interchangeable on dosage-response curves, laser power was scanned at all tested flow rates. Errors from the calibration curve were then calculated.

Fluorescence intensities were corrected by subtracting buffer-only background measurements. Importantly, we found that the background fluorescence was independent of h, which suggests that the PDMS was not deforming under the range of pressures we consider, since any such change would alter the geometric factors associated with light collection. Dosage was determined from height-corrected flow measurements and transmitted laser power. Master curves were then generated from convex analysis as described elsewhere.[23]

Validating measurements below 10 nL/min. A fundamental claim of this work is the experimental result that our optofluidic flow meter can achieve accurate, in situ, and continuous measurement to 10 nL/min and below. By our understanding, there is no technique capable of continuously measuring flows below 10 nL/min scale with low uncertainty, so we rely on a new method of zero-flow determination to precisely estimate the lower bound of flow measurement.

For the purposes of stability and reliability, gravity-based flow controllers are among the simplest in that flow rate is determined by the linear relationship $dh = (h - h_0) = v_v\mathcal{R}/\rho g_n$, where dh is the height relative to a reference height, h_0, (height where $v_v = 0$), $\mathcal{R}$ is the resistance to flow, and g_n is standard acceleration due to gravity. Thus, the absolute accuracy about h_0 determines the relative accuracy in v_v as $h \to h_0$. We use the zero-flow measurement technique to identify h_0 and to calibrate the gravity-based flow controller (**Suppl. Info. 2**). Without the zero-flow measurement, we cannot determine h_0 by extrapolating measurements performed at non-zero flows, as the uncertainty in h_0 will grow by a lever arm effect (see **Suppl. Info. 3**).

RESULTS

Optical characterization of the device. In general for optofluidic devices, and particularly for this device, it is important

to maintain efficient delivery and collection of light from a region of interest in the microchannel. Though we have not undertaken a thorough study to optimize light throughput, we offer some design considerations and performance metrics. To improve light transmission through the optical waveguides and reduce light leakage due to waveguide roughness,[26] we found that it was important to create smooth channel sidewalls. High-resolution laser writing of either chrome masks (prior to photolithography) or direct writing of SU8 on silicon led to waveguides of high transmission efficiency. In addition, to minimize leakage of excitation light into the emission waveguide, microchannels were added between waveguides and filled with black PDMS (Sylgard 170). Importantly, these structures prevent unwanted photobleaching of fluorescein outside the interrogation region, which increases the characteristic length of the channel and reduces the Peclet number.

The previously discussed design requirements imply that the length of the laser profile (in z) is an important factor in determining low-flow performance. Practically, the minimum microchannel height is about 80 μm, which is the smallest channel (with a 300 μm wide opening) that can accommodate a standard optical fiber (125 μm diameter). The laser profile was maintained to the same characteristic dimension by narrowing the waveguide and adding a lens to the end. Some widening due to optical aberrations in the system is still visible (see **Figure 1D**).

We acquire background fluorescence measurements of buffer-only flow to estimate the efficiency of our waveguides and to account for excitation light reaching the fluorescence meter and absorbance of excitation light through the channel. For 60 mW input power (corresponding to approximately 17 mW at the end of the fiber into the device), we recorded between 1 and 4 mW at the output of the transmission fibers in either the narrow (25 μm; **Figure 1B**) or wide (100 μm; **Figure 1C**) interrogation channels, indicating roughly 6−24% transmission efficiency through the system. We did not find systematic dependence on channel width, though one might expect slightly lower transmission efficiency in the 100 μm channel because of the longer path length. Similarly, we measured a reflected power of <400 pW in the emission waveguide, which corresponds to an excitation−rejection ratio of >106:1. This background contribution is as much as 10% of measured optical power at highest dosages in this study (60 mW laser, 4 nL/min flow), but for measurements above 25 nL/min, it is less than 1% of the signal. Nonetheless, all fluorescence measurements were corrected for background buffer emission.

Determination of zero flow. Expanding relative uncertainties as flow rates approach zero are an inherent limitation of traditional flow meters.23 Errors due to factors such as evaporation, diffusion, or capillary forces and lack of precision in system geometry become ever increasing as scales diminish. The optofluidic flow meter has a unique ability to provide contrast between pressure-driven convective flow and diffusion at near-zero flows. At zero flow, all molecules in the interrogation region photobleach quickly, but a steady (and equal) diffusion of unbleached molecules from both sides of the interrogation region dictates a critical fluorescence value. Estimation of zero flow with the optofluidic flow meter is accomplished by finding the bounds of reservoir height at which the fluorescence signal reaches its critical value, which happened to be a minimum. This phenomenon was validated visually by watching the pattern of photobleaching as the flow shifts from positive to negative bias in the interrogation region (**Figure 2**). A slight positive flow replenished fluorescein on the upstream side (e.g., brightening on the left); a slight negative flow replenished fluorescein on the downstream side (e.g., brightening on the right). With very low flows, care must be taken to refresh the fluorescein between each height to ensure unbleached fluorescein is available on both sides of the interrogation region.

Initially we conducted measurements with only one waveguide to collect fluorescence emission and determined it was most sensitive when placed on the upstream side of the excitation waveguide. We realized that there could be some bias in finding the minimum fluorescence signal because the waveguide may not collect fluorescence uniformly or totally. Therefore, we modified our device to have symmetric fluorescence collecting waveguides upstream and downstream of the excitation waveguide. Using the waveguides independently, it is possible to determine the polarity of flow.

By finding symmetry in photobleaching by imaging, we found that we could repeatably determine the height of the water column corresponding to zero flow (h_0) to within ± 0.25 mm ($\delta h_{0,100\mu m}$, which we take to be the standard deviation for a normal distribution) on a 100 μm wide flow region **(Figure 2A)** and to within ± 0.05 mm ($\delta h_{0,25\mu m}$) on a 25 μm flow channel **(Figure 2B)**. Using thresholding around the minimum fluorescence signal collected by symmetric waveguides (**Figure 2C**), we estimate a height uncertainty to within ±0.8 mm on a 100 μm wide flow region and to within ±0.26 mm on a 25 μm flow channel. We expect the imaging data to be more sensitive, as much more emitted light is captured by the microscope lens than the waveguides. More rigorous analysis, including summing the fluorescence from both waveguides, could reduce the uncertainty of the power meter measurements.

Using a Sensirion flow meter calibrated to 5 % uncertainty by a gravimetric calibration system[11] at two heights, where $h_2 \to v_{v2} = 0$, we determined from **Suppl. Eq. 6 (Suppl. Info. 2)**, the conductance ($1/\mathcal{R}$) of the system to be ≈ 0.26 nL/min/Pa (which corresponds to 2.5 nL/min *per* mm of water column height change). Importantly, restating the result from **Suppl. Eq. 8**, accurate determination of the device conductance depends primarily on the accuracy of the flow meter used to calibrate the system at high flow rates.

From **Figure 2C** and **Suppl. Eq. 9**, we find that the optofluidic flow meter can achieve roughly ± 0.63 nL/min or ± 2 nL/min uncertainty around zero flow from a 100 μm wide region using imaging or power measurements, respectively. For the 25 μm region, uncertainties were as low as ± 0.13 nL/min or ± 0.65 nL/min from imaging or power measurements, respectively.

Interpolation between a measurement on the calibrated meter to the zero-flow measurement point can be used to achieve 5.5 % uncertainty in flow measurements to 28 nL/min from waveguide collection measurements or as low as 5.7 nL/min with imaging in the narrow region. Flow uncertainties below 10 % can be maintained to 7.5 nL/min or 1.5 nL/min using measurements from waveguides or imaging, respectively. Thus, as part of a height-corrected flow controller, we believe it is reasonable to conclude that the current configuration of the optofluidic meter is suitable for flow measurement down to ≈ 2 nL/min. **Figure S1B** shows a plot of the relative uncertainties achievable using the 25 μm channel to calibrate the reservoir height. For comparison, an extrapolation using only a calibrated commercial meter with measurements at 367 nL/min and 738 nL/min, goes above 10 % uncertainty below 240 nL/min.

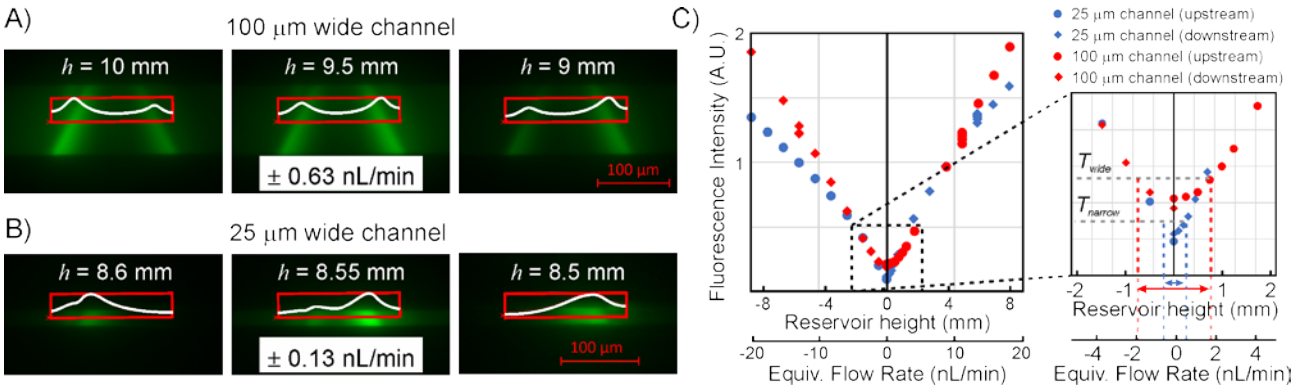

Figure 2. Determination of uncertainty in height around zero flow. Microscopy images show fluorescence intensity (green) at different heights near zero flow in wide (A) and narrow (B) channel interrogation regions. The white curve shows a line scan of fluorescence intensity across the illumination region (along the bottom line of the red box). When flow is near zero, all fluorescein in the channel is bleached, except for fresh fluorescein diffusing into the edges of the laser path. Brighter intensity on the left is used to indicate positive flow, brighter intensity on the right indicates negative flow. Zero flow is a point somewhere between. (C) Steady-state fluorescence values from waveguides upstream (equivalent to being positioned on the left in the images) and downstream (right in the images) of the excitation beam are shown for the two microchannel widths at different heights of the fluid reservoir (e.g., the flow controller). The equivalent flow rate was determined from the conductance of the system (2.5 nL min^{-1} mm^{-1}). Inset shows magnification of the critical region and application of thresholds, T_{wide} and T_{narrow} (gray dotted lines), to isolate the minimum of the signal and determine the height, and corresponding flow, uncertainty ((blue dotted lines show 25 μm channel; red dotted lines show 100 μm channel).

Fluorescence-dosage calibration curve. Fluorescence efficiency measurements were collected using 50 μmol/L fluorescein solution flowing through the 100 μm wide interrogation region. The first tested device had only a single upstream fluorescence collection waveguide. We adjusted the height to achieve a flow rate (165 nL/min) that was near the limit of 5 % uncertainty for a commercial flow meter. Emitted fluorescence intensity was collected over input laser powers ranging from 3 mW to 60 mW in 3 mW increments (**Figure 3A**). Laser power in the dosage calculation was converted to an effective excitation power to account for nonlinear dependence of photobleaching on laser power, which we empirically determined to be a power factor 1.18 [i.e., $f(p) = p^{1.18}$]. To achieve approximately 10-foldlower dosages with our laser system, which has limited stability below 3mW output power, we integrated a 10 % neutral density filter (transmission efficiency at 488 nm measured as 8.4 %). These lower power data allow fluorescence measurements to be bootstrapped to higher flow rates, which although are not an improvement over existing flow meters, they enable the optofluidic meter to span a broader range of flows.

A master dose-response curve was generated from the 165 nL/min flow data using a convex regression method as described in our previous manuscript.[23] Fluorescence measurements were then collected by scanning laser powers at lower flow rates (lower reservoir heights) and scaled using zero-flow correction, as described above. Dosage response curves were determined for each flow rate and compared to the master curve in regions of overlap, as shown in **Figure 3B**. **Figure 3B inset** shows the relative error for each measurement, which is the difference from the master curve divided by the flow rate at that dosage. Overall, data were agreement with the master curve to within
4 % relative error down to 27.3 nL/min, the lowest flow with dosages that overlap with the 165 nL/min master curve. Though we cannot evaluate agreement of flow rates below 27.3 nL/min, it is instructive to see that they appear as continuous extensions of the master curve to the 4 nL/min data points (**Figure 3B**), as determined by the flow controller settings. This suggests that the 100 μm channel is useful as a flow-meter to this scale, which would achieve a previously unattainable measurement capability for a continuous flow meter.

We next tested estimation of flow rates from dose-response scaling using a device having symmetric waveguides placed on each side of a narrow (25 μm) and wide (100 μm) channel passing through an interrogation region. **Figure 3C** shows fluorescence efficiency data (the sum of both collection waveguides for each region) collected by scanning excitation laser intensity at various flow rates. **Figure 3C inset** shows the relative error from a master curve including data from 50 nL/min to 800 nL/min. Relative errors were maintained below 5% to 43 nL/min and almost to 23 nL/min (5.4%).

A 100 μm wide interrogation with symmetric collection waveguides was also measured as above (**Figure 3D**). The wider channel contains more fluorescein and thus has a larger fluorescence signal than the narrow waveguide. The relative errors of the flow measurements using the wider region are shown in **Figure 3D inset.** Relative errors were maintained below 5 % to 10 nL/min. These data are discussed in the limitations and open questions section 2, below.

Comparison of Expected Theoretical and Observed Performance. Flow measurements in the optofluidic devices are based on the excitation and emission of fluorescein molecules as they flow through the interrogation region, but the measurement signal, *per se*, is the *loss* of fluorescence due to photo-destruction of the molecule based on the integrated light energy it receives. Slower flows or more powerful excitation light will bleach fluorescein before it fully crosses the interrogation region, thus lowering the total fluorescence measured by the emission detector. Photomicrographs of this phenomenon demonstrate loss of fluorescence and reduction in penetration depth as flow rate decreases (**Figure 1D**).

As flow rate approaches zero, the signal reaches a minimum – the point at which the timescale of diffusive motion of the

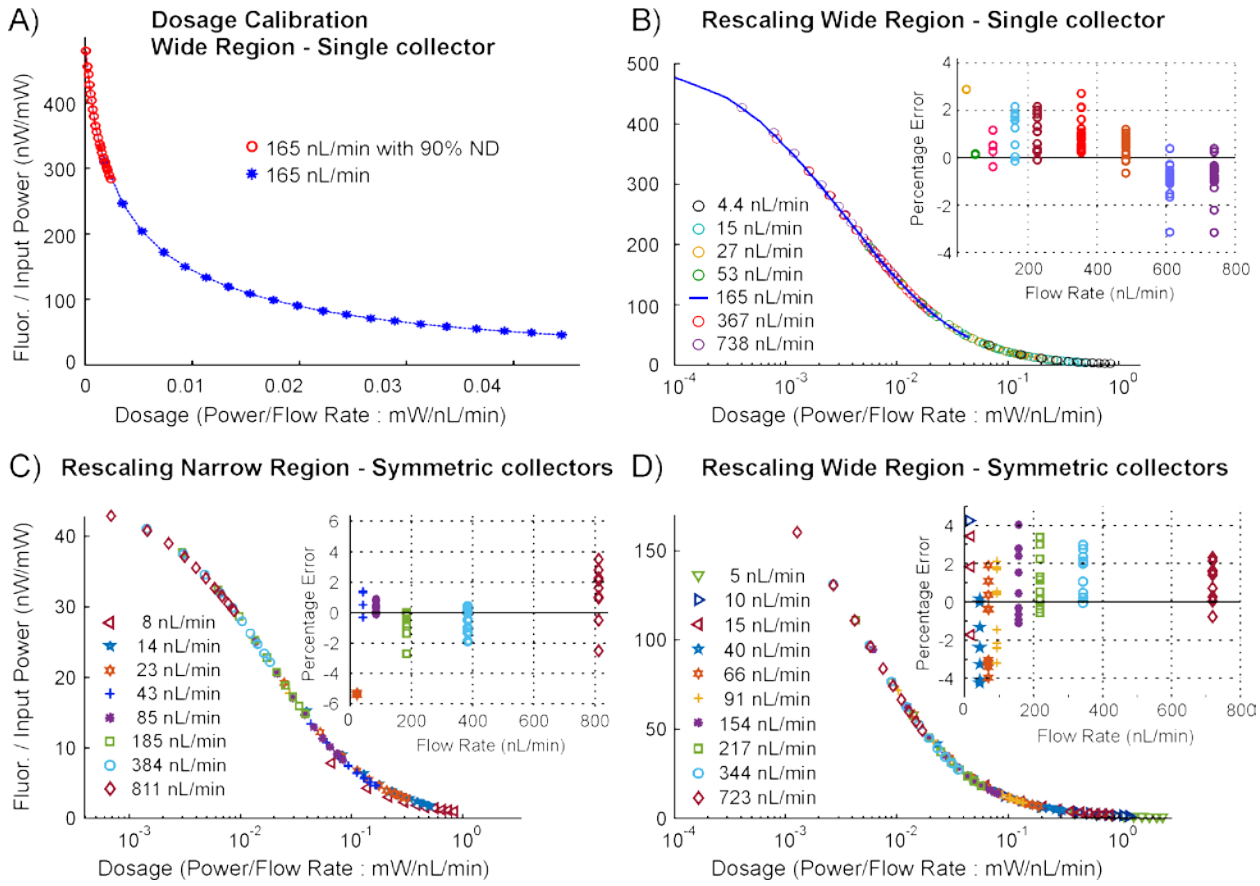

Figure 3. (A) Dosage curves for a 100 µm wide interrogation region with a single upstream collector waveguide. Blue curve represents data taken with laser power scanned from 3 mW to 60 mW. The red curve indicates the same laser scan, but with device preceded by a nominal 90 % neutral density (ND) filter. (B) Fluorescence efficiency data for laser power scans at different flow rates are compared to the 165 nL/min master curve, which includes both data sets from (A) (blue line). (C) Dosage curves for a narrow (25 µm wide) interrogation region with symmetric fluorescence collector waveguides on both sides of the excitation laser. (D) Dosage curves for a wide (100 µm wide) interrogation region with symmetric fluorescence collector waveguides on both sides of the excitation laser. Fluorescence data shown in (C) and (D) are sum of intensities from both collectors. Data in (B), (C), and (D) are shown with log(x-axis) to facilitate visualization over the 4 orders of magnitude in dosage. **Insets** of (B), (C), and (D) show relative errors in flow based on the deviations from the master curves of the respective data sets.

molecules dominates convection. This lower limit can be assessed with the Peclet number. Demonstration of the expected separation of convection from diffusive "smearing" of the signal is plotted in **Figure S1A**. Assuming a fixed 100 µm interrogation region, we expect uncertainties in flow to remain within 5 % and 10 % flow uncertainty at 50 nL/min and 25 nL/min, respectively. Errors in the scaling relationship overperform what is expected from the simple analysis presented above. This is likely because the characteristic microchannel dimensions in the *Pe* calculation are an overestimate of the actual size of the fluorescing region, which becomes considerably reduced at high dosages due to photobleaching; see **Figure 1D**. Thus, it is more appropriate to define the Peclet number in terms of some reduced critical dimension, $L_a(v_y)$, where L_a is reinterpreted as the critical dimension of the fluorescing region and having the property that $L_a \ll L_z$ when $v_y \to 0$. For the time being, determination of L_a is an open problem, but an estimate can be obtained from **Figure 1D**, which can provide some lower bound on the critical dimension of the system. Specifically, the maximum extent of fluorescence at several flow rates are shown overlaid on **Figure S1A**. Using these measurements as indicators of the critical dimension for diffusion, we estimate that best-cases for 5 % and 10 % flow uncertainties would be about 10 nL/min and 5 nL/min, respectively. One can also use **Figure S1A** to make judgements about the expected performance of different flow meter designs. Reducing channel width, height, or cross-section of the laser could further reduce uncertainties for low flow rates. One tradeoff to consider, however, is that reduced dimensions of the interrogation region lead to proportionally smaller fluorescence signals, which effectively increase uncertainty in the measurement system.

DISCUSSION AND CONCLUSION

Whereas most flow meters suffer from expanding uncertainties as flow decreases, our optofluidic flow meter provides two independent approaches to measuring low flows while preserving the relative uncertainties of higher (calibrated) flow rates into a lower range. We find that the combined methods enable achievement of dynamic flow measurements with 5% uncertainty down to the order of 10 nL/min. Importantly, neither technique requires a microscope, which facilitates portability given integration of on-chip light sources and detectors.

Our methods require a calibrated flow meter to determine the fluidic resistance of the chip and to reference the master curve to a known flow rate through a dosage relationship. However, once a flow meter is calibrated and its conductance calculated, it can be used to set up a high-precision pressure driven flow controller. Other devices with known conductances can then be substituted into the flow controller network. Flow measurements can then be corrected as $v_v^* = v_v\, C2/C1$, where $C1$ and $C2$ are the conductances of the meter and second microfluidic device, respectively. The limits regarding interchangeability of such a system would need to be evaluated, particularly if it were meant to be used without continuous flow measurement or regular recalibration. If one was able to maintain a known fluidic resistance or to determine changes in fluidic resistance dynamically, it would be possible, given accurate pressure control, to independently operate the optofluidic meter without need of a commercial meter or calibration system. Although it is unclear if uncertainties are sufficiently low, pressure drop methods[27] and electrical impedance-based methods could provide promising alternatives to calibration and monitoring of fluidic resistance.[28,29]

Comparison with other flow measurement methods. Fluorescent molecules have previously been utilized in several flow measurement techniques.[21,22,30−33] However, these approaches generally rely on time-of-flight measurements between two points in a device and/or detailed modeling assumptions that are hard to validate. Current strategies to determine flow rates by such means require microscopy, image processing, and accurate knowledge of the system geometry. Importantly, such techniques are especially susceptible to model-form errors that arise when uncertainties in assumptions about the details of the system propagate into the final measurements. For example, in early work using photobleaching at a single laser crossing, Sugarman and Prud'homme[21] develop multiple empirical models relating fluorescence intensity (scaled by mean velocity) to flow velocity (scaled by a photobleaching rate constant). Although it appears that flow rates on the order of 5 nL/min are realized, it is instructive to observe nearly 30% spread in their reduced fluorescence measurements at low flows. Mapping that back to the flow rate axis likely results in very large relative errors in estimates of flow from a measured fluorescence intensity. While difficult to know for certain, we speculate that such errors arise from uncontrolled model-form uncertainty. In particular, note that the measurements of Sugarman and Prud'homme require a choice of which model to use for the purposes of analyzing data. As none of these may be a good representation of the system, their analysis introduces inherent errors that can be difficult to quantify. Indeed, such model-form uncertainty can entirely dominate a measurement. See the companion theory paper for a mathematically rigorous justification of our scaling relationship and its reduction in model-form uncertainties.[23]

Notably, Flamion et al.[33] also demonstrate biological relevance of nanoflow measurement by tracking movement of a bleached plug of fluorescein in an isolated kidney tubule. They show measurements in the range of 4−40 nL/min with stated 10% accuracy. This method did not include a calibrated comparison or uncertainty analysis, which means that absolute errors could be larger.

In a later paper, Wang[22] used a polynomial fit to interpolate the relationship between fluorescence intensity and flow rate down to the order of 20 nL/min with a standard deviation of ≈4%. While seemingly accurate, this paper does not compare flow measurements to a calibrated approach or develop a robust uncertainty analysis. Moreover, the use of a polynomial is less physically informed than the models of Sugarman and Prud'homme21 and possibly subject to larger model-form uncertainties. It is well-known that empirical polynomial fits cannot be used to extrapolate data or measurements; thus, the technique is limited to the range of the detector used for calibration. In contrast, our method allows for a decade or more of extrapolation. In our setup, we have virtually no detailed information about the system; channel dimensions, the shapes of the flow and laser profiles, and collection efficiencies of waveguides are unknown. Thus, model-form errors would entirely overwhelm our measurements had we attempted to analytically characterize the raw signals; see our complementary manuscript.[23]

Nonetheless, we can safely leverage several generic but critical pieces of information to perform extremely robust measurements: (i) the system parameters (e.g., geometry, laser profiles, etc.) are constant, and (ii) dye molecules on average bleach after a fixed number of fluorescence events.18 Thus, the same number of bleached molecules should arise from either increasing the photon flux (power of excitation beam) or the dwell time (1/flow velocity) of the dye molecules, at least while diffusion is an insignificant contributor to velocity. As a result, we can determine the master curve experimentally by varying the laser power for fixed (known) flow rates. Conceptually, this approach can be viewed as a physics-based extrapolation method for extending the domain of validity of an independent, established flow measurement. As opposed to more common extrapolation techniques (e.g., based on polynomial regression), however, our approach scales down the independent measurement of flow and its uncertainties.[23] Thus, we arrive at the counterintuitive conclusion that the optofluidic device decreases the absolute scale of uncertainty of another flow meter below the latter's domain of validity. Thus, both flow meter and flow controller have uncertainties that are largely dictated by the quality of the independent calibration tool. We expect that greater precision in both can be achieved by directly calibrating our system to a gravimetric standard.[11]

On the Independence of the Flow Controller. An important theme underlying this work is the recognition that validation of a measurement method operating in new regimes (in our case, less than 100 nL/min) requires a separate measurement and/or control technique for the purposes of comparison. In our case, at zero flow, the optofluidic device uses a distinct operating principle based on determination of a critical point, which requires no calibration. Because all other measurements at nonzero flow rates rely on a different scaling argument and separate calibration, the zero reference is therefore determined independently.

Limitations and Open Questions

1. Sensitivity of the zero-flow measurement. Estimation of critical fluorescence value to determine zero flow depends on the symmetry of the detection system. Further, the concentration of unbleached fluorophore on either side of the illumination region is sensitive to the flow history and limits the utility of continuous operation of the laser for very low flow measurements, particularly if the polarity of the flow changes. Improving the estimation of zero flow may be possible by decreasing the width of the flow channel or increasing the fluidic resistance. In addition, using fluorescein-functionalized

molecules with greater mass (lower diffusion coefficients) would also improve discrimination of convection and diffusion.

2. Using a narrower interrogation region for dosage scaling. As expected from increased linear velocity for a given flow rate, the narrower, 25 μm wide interrogation region was better able to distinguish pressure-driven flow from diffusion, as demonstrated in **Figure 2C**. The narrower region was also found to be more sensitive to lower volumetric flow rates, as demonstrated by a shift in the steepest part of the dosage-response curve to the right (**Figure 3C**). With faster linear velocities, dyes endured longer in the interrogation region for a similar excitation power and volumetric flow rate. Indeed, this phenomenon was seen in increased sensitivity of the narrower region to near-zero flow rates (**Figure 2C**). The dosage−response curves for the narrower region, as compared to the wider, 100 μm region, show a break from the main trend at 8 nL/min. Larger relative errors in the narrow region are expected given larger relative contribution of background and higher noise compared to the lower fluorescence intensities in the narrow region. More careful studies are needed to determine sources of error in these very small flow rates.

3. Uniqueness of each device. The relationship between fluorescence efficiency and dosage is unique to each assembled device and is likely to vary due to subtle differences in the system geometry and waveguide efficiency resulting from fabrication. Replica molding of PDMS has generally high fidelity and is not likely to lead to large variability in system geometry; we suspect that device-to-device variability is likely largely a function of the quality of the filled waveguides and the coupling efficiency of the inserted fiber-optic cables.

We have not undertaken a full study of the reproducibility of optical efficiency through individually fabricated devices, nor have we carefully studied changes in device performance over time. Though important, such topics are beyond the scope of this manuscript and are the subject of future study. Briefly, we expect variation in optical efficiency of the device could be caused by differences in fiber insertion depth and angle, roughness in microchannel walls, impurities in the optical adhesive, fiber-to-fiber coupling efficiency, and, to a lesser extent, completeness in curing of optical adhesive or PDMS (which can affect refractive index),[35] variations in optical fiber length (we use fibers ranging from 0.5 to 2 m long), and device aging.

4. Dependence on fluorophore. Fluorescein is highly susceptible to photobleaching,[20] which enables the device to achieve high contrast over a range of dosages corresponding to nanoliter-per-minute flow rates. For concentrations well below self-quenching, higher concentrations of fluorescein give brighter signals over background, but the choice to go too high in concentration runs the risk of contaminating the flow system or adding additional background signal to other fluorescent species that might also be measured in the flow. As concentration is lowered, noise becomes more significant, and the uncertainty of fluorescence efficiency increases. Regarding reproducibility, fluorescein emission is sensitive to environmental factors, such as pH,[36] so care must be taken to maintain buffer conditions and restrict sample exposure to light. These factors make day-to-day comparability of master curves dependent on the ability to prepare and maintain equivalent fluorescein solutions. We also note that fluorescein is charged and is likely to migrate in the presence of an electric field in the channel. A neutral fluorophore may be preferred for such applications. These issues are the focus of future work, as we continue to refine the method to be more robust, more versatile and user-friendly, and more accurate.

ASSOCIATED CONTENT

Supporting Information.

The Supporting Information is available free of charge on the ACS Publications website at DOI: 10.1021/acs.analchem.9b02056.

Details of Re number calculation, calculations for relative uncertainty in volumetric flow based on the Peclet number, and performance specifications for gravity-based flow control (PDF).

AUTHOR INFORMATION

Corresponding Author

*Tel. 301-975.5529. Email: gregory.cooksey@nist.gov

Notes

The authors declare no competing financial interest.

ACKNOWLEDGMENT

We acknowledge gravimetric calibration of the commercial flow meter by James Schmidt and John Wright. The authors would like to thank Michael Moldover, John Wright, and James Schmidt for useful discussion.

REFERENCES

(1) Heemskerk, A.A.M.; Busnel, J-M.; Schoenmaker, B.; Derks, R.J.E.; Klychnikov, O.; Hensbergen, P.J.; Deelder, A.M.; Mayboroda, O.A. *Anal. Chem.*, **2012**, 84, 4552-59.

(2) IEC TC/SC 1998 Particular requirements for the safety of infusion pumps and controllers. IEC 60601–2–24 Ed. 1.0.

(3) ISO 2010 Infusion equipment for medical use ISO 8536–1 to 12.

(4) ISO 2010 Medical devices—non-electrically driven portable infusion devices ISO 28620:2010.

(5) Zhang, J.; Coulston, R.J.; Jones, S.T.; Geng, J.; Scherman, O.A.; Abell, C. *Science*, **2012**, 335, 690-694.

(6) Kim, S.; Kim, H.J.; Jeon N.L. *Int. Biol.*, **2010**, 2, 584-603.

(7) Pamme, N. *Lab Chip*, **2007**, 7, 1644-59.

(8) Beebe, D.J.; Mensing, G.A.; Walker, G.M. *Annu. Rev. Biomed. Eng.*, **2002**, 4, 261−286.

(9) Kovarik, M.L.; Ornoff, D.M.; Melvin, A.T.; Dobes, N.C.; Wang, Y.; Dickinson, A.J.; Gach, P.C.; Shah, P.K.; Allbritton, N.L. *Anal. Chem.*, **2013**, 85, 451−472.

(10) Melvad, C.; Kruhne, U.; Frederiksen, J. *Meas. Sci. Technol.*, **2010**, 211-6.

(11) Schmidt, J.W.; Wright, J.D. *Proc. 9th Int. Symp. Fluid Flow Meas.*, **2015**, 14-17.

(12) Bissig, H.;Petter, H.T.; Lucas, P.; Batista, E.; Filipe, E.; Almeida, N.; Ribeiro, L.F.; Gala, J.; Martins, R.; Savanier, B.; Ogheard, F.; Niemann, A.K.; Lötters, J.; Sparreboom, W. *Biomed. Eng.-Biomed. Tech.*, **2015**, 60, 301-16.

(13) Ahrens, M.; St. Klein; Nestler, B.; Damiani, C. *Meas. Sci. Technol.*, **2014. 25, 1-9.**

(14) Westin, K.J.A.; Choi, C.-H.; Breuer, K.S. *Exp. Fluids*, **2003**, 34, 635-42.

(15) Kuo, J.T.W.; Yu, L.; Meng, E. *Micromachines*, **2012**, 3, 550-73.

(16) Salipante, P.; Hudson, S.D.; Schmidt, J.W.; Wright, J.D., *Exp. Fluids*, **2017,** 58, 85.

(17) Sadeghi, J., Ghasemi, A.M.B.; Latifi, H. *Lab Chip*, **2016**, 16, 3957-68.

(18) Hirshfeld, T. *Appl. Optics*, **1976**, 15, 3135-9.

(19) Song, L.; Hennik, E.J., Young, I.T., Tanke, H.J. *Biophys. J.*, **1995**, 68, 2588-2600.

(20) Patterson, G.H.; Piston, D.W. *Biophys. J.*, **2000**, 78, 2159-52.

(21) Sugarman, J.H.; Prud'homme, R.K. *Ind. Eng. Chem. Res.* **1987**, 26, 1449-1454.

(22) Wang, G.R. *Lab Chip*, **2005**, 5, 450-456.

(23) Patrone, P.N.; Cooksey, G.A.; Kearsley, A. “Dynamic measurement of nanoflows: theory and analysis of an optofluidic flowmeter,” *Phys. Rev. Appl.*, **2019**, 11, 034025.
(24) McDonald, J.C.; Duffy, D.C.; Anderson, J.R.; Chiu, D.T.; Wu, H.; Schueller, O. J.A.; Whitesides, G.M. *Electrophoresis*, **2000**, 21, 27-40.
(25) Cooksey, G.A.; Sip, C.G.; Folch, A. *Lab Chip*, **2009**, 9, 417-26.
(26) Lee, K.K.; Lim, D.R.; Luan, H.-C.; Agarwal, A.; Foresi, J.; Kimerling, L.C. *Appl. Phys. Lett.*, **2000**, 77, 1617-19.
(27) Kim, D.; Cheslerab, N.C.; Beebe, D.J. *Lab Chip*, **2006**, 6, 639-44.
(28) Niu, P.; Nablo, B.Jl; Bhadriraju, K.; Reyes, D.R. *Anal. Chem.*, **2017**, 89, 11372-77.
(29) Godwin, L.A.; Deal, K.S.; Hoepfner, L.D.; Jackson, L.A. Easley, C.J. *Anal. Chim. Acta*, **2013**, 758, 101–107.
(30) Ross, D.J.; Johnson, T.J.; Locascio, L.E. *Anal. Chem.*, **2001**, 73 (11), 2509-15.
(31) Mosier, B.P.; Molho, J.I.; Santiago, J.G. *Exp. Fluids*, **2002**, 33, 545-54.
(32) Schrum, K.F.; Lancaster III, J.M.; Johnston, S.E.; Gilman, S.D. *Anal. Chem.*, **2000**, 72, 4317-21.
(33) Flamion, B.; Bungay, P.M.; Gibson, C.C.; Spring K.R. *Biophys. J.*, **1991**, 60, 1229-1242.
(34) Sharma, P.; Motte, J.-F.; Fournel, F.; Cross, Bl; Charlaix, E.; Picard, C. *Nano Lett.*, **2018**, 18, 5726-5730.
(35) Chang-Yen, D. A.; Eich, R.K.; Gale, B.K. *J. Lightwave Technol.*, **2005**, 23, 2088-2093.
(36) Sjöback, R.; Nygren, J.; Kubista, M. *Spectrochimica Acta A*, **1995**, 51, L7-L21.